Article

Current Biology

Non-linear stress-softening of peptidoglycan mediates bacterial cell shape homeostasis

Graphical abstract

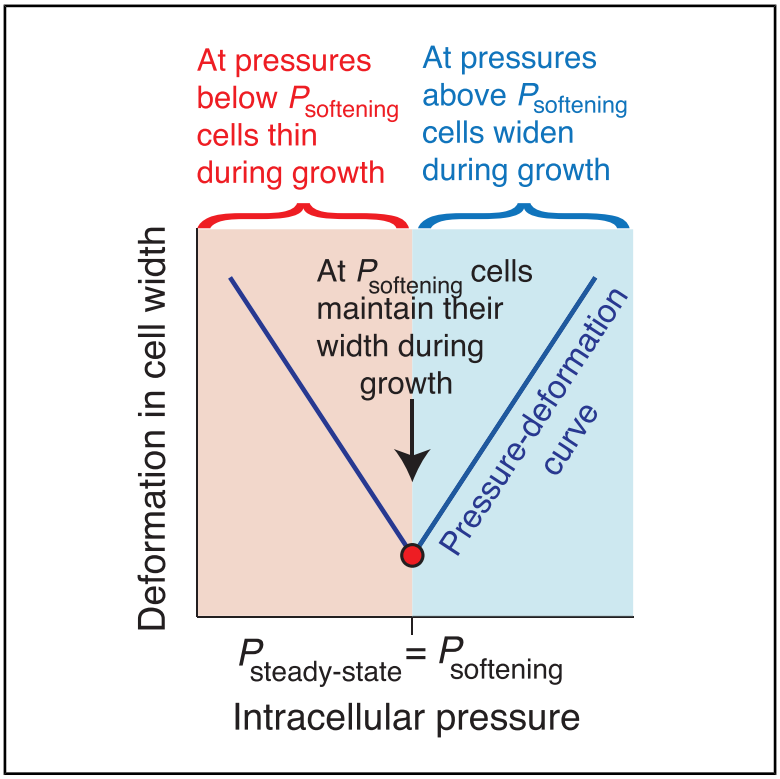

Highlights

- The Gram-positive bacterial cell wall exhibits stress-stiffening and -softening
- During cell growth, the wall is inflated to the critical stress-softening pressure
- Elasticity theory explains why this results in growth at a constant cell width

Authors

Paola Bardetti, Felix Barber, Dylan Fitzmaurice, Enrique R. Rojas

Correspondence

rojas@nyu.edu

In brief

Bardetti et al. find that the cell wall of rod-shaped Gram-positive bacteria exhibits an acute non-linearity in its mechanical properties. By inflating themselves, precisely, to the critical pressure at which this non-linearity occurs, cells achieve growth at a constant width.

Bardetti et al., 2026, Current Biology *36*, 1156–1165
March 9, 2026
https://doi.org/10.1016/j.cub.2026.01.043

CellPress

CellPress
OPEN ACCESS

Current Biology

Article

Non-linear stress-softening of peptidoglycan mediates bacterial cell shape homeostasis

Paola Bardetti,[1] Felix Barber,[1] Dylan Fitzmaurice,[1] and Enrique R. Rojas[1,2,*]
[1]Department of Biology, New York University, 12 Waverly Place, New York, NY 10003, USA
[2]Lead contact
*Correspondence: rojas@nyu.edu
https://doi.org/10.1016/j.cub.2026.01.043

SUMMARY

The bacillus—or rod—is a pervasive cellular morphology among bacteria. Rod-shaped bacteria elongate without widening by reinforcing their cell wall anisotropically, along the cell's circumference, but it is unknown how cells prescribe the specific degree of anisotropy that ensures growth at a constant, target width. Through super-resolution measurements of cell wall mechanical properties, we discovered that the *Bacillus subtilis* cell wall exhibits non-linear stress-stiffening and stress-softening exclusively in the circumferential direction. Furthermore, during steady-state growth, the cell wall is inflated precisely to the acute non-linearity corresponding to softening. Elasticity-based theory explains why this results in cell growth at a constant width. Finally, dynamic measurements of the non-linear mechanical properties during cell-width adaptation identified a negative-feedback system that regulates width homeostatically through tuning of both intracellular pressure and the critical pressure of the non-linearity. In other words, the cell wall is an "adaptive material" whose exotic mechanical properties are exquisitely engineered to execute cellular morphogenesis.

INTRODUCTION

The peptidoglycan cell wall is a covalently cross-linked polymer network that defines the size and shape of bacterial cells (Figures 1A and 1B). Three processes mediate expansion of the wall during cell growth: peptidoglycan synthesis,[1] enzymatic hydrolysis of the peptide moieties,[2] and mechanical deformation of the wall by the large intracellular turgor pressure[3] (≈ 1–30 atm, depending on species[4,5]). The primary protein machinery that executes peptidoglycan synthesis during the growth of rod-shaped bacteria is the multiprotein Rod complex, which is scaffolded by prokaryotic homologs of actin.[6–8] Rod complexes synthesize peptidoglycan processively, resulting in anisotropic cell wall microstructure in which the glycan moieties are oriented, on average, parallel to the cell's circumference (θ; Figures 1A and 1B)[9] and are connected to one another via the peptide moieties. It is believed that the oriented glycan polymers promote rod-shaped growth by mechanically reinforcing the cell wall along its circumference, effectively "girdling" the cell in this dimension[10] (Figures 1A and 1B). It is also commonly assumed that peptides are oriented longitudinally[11] (l; Figure 1A). If this were so, hydrolysis of load-bearing peptides would promote cellular elongation rather than widening.

This model, however, is not sufficient to explain rod-shaped morphogenesis. Glycans are not oriented strictly circumferentially[9] (Figure 1B), nor are they infinitely stiff.[4] Similarly, peptides are not oriented strictly longitudinally, and in Gram-positive bacteria, the requirement for peptides to connect glycans across the thickness of the cell wall makes this impossible. Finally, inflation of the cell by turgor pressure causes anisotropic surface tension in the cell wall whereby the circumferential tension is approximately twice the longitudinal tension[12] ($\lambda_\theta = 2\lambda_l$; Figure 1A). Therefore, based on first principles, hydrolysis of peptide moieties during cell growth is expected to lead to both elongation and widening.

In this light, it is not understood how rod-shaped bacteria avoid widening or how they tune the structure of the cell envelope to control cell width, which they do with ≈40 nm precision (±5%; Figure S1A). Here, we describe how the Gram-positive bacterium *Bacillus subtilis* achieves width homeostasis through a sharp non-linearity in the anisotropic mechanical properties of its cell wall. More specifically, we found that the cell wall exhibits both stress-stiffening and stress-softening, leading to distinct regimes of intracellular pressure in which inflation of the cell causes either cell widening or constriction. Cells maintain a constant cell width by inflating themselves precisely to one of the boundaries between these regimes. Finally, we demonstrate how the bacteria adaptively manipulate these strange mechanical properties to achieve cell width homeostasis.

RESULTS

Peptide hydrolysis causes cell widening

To explicitly test whether peptidoglycan hydrolysis leads to cell widening, we measured the change in cell width immediately after exogenous digestion of cell wall peptides in the Gram-positive bacterium *Bacillus subtilis*. We effected hydrolysis by using microfluidics to acutely perfuse exponentially growing bacterial cells with a purified recombinant amidase derived from the lytic bacteriophage SPP1[13] (Figure 1A) and measured changes in cell width with <20 nm resolution at the single-cell level and <10 nanometer resolution at the population level, using a fit-free super-resolution method that we developed (Figures 1C and 1D; STAR Methods). As hypothesized,

CellPress
OPEN ACCESS

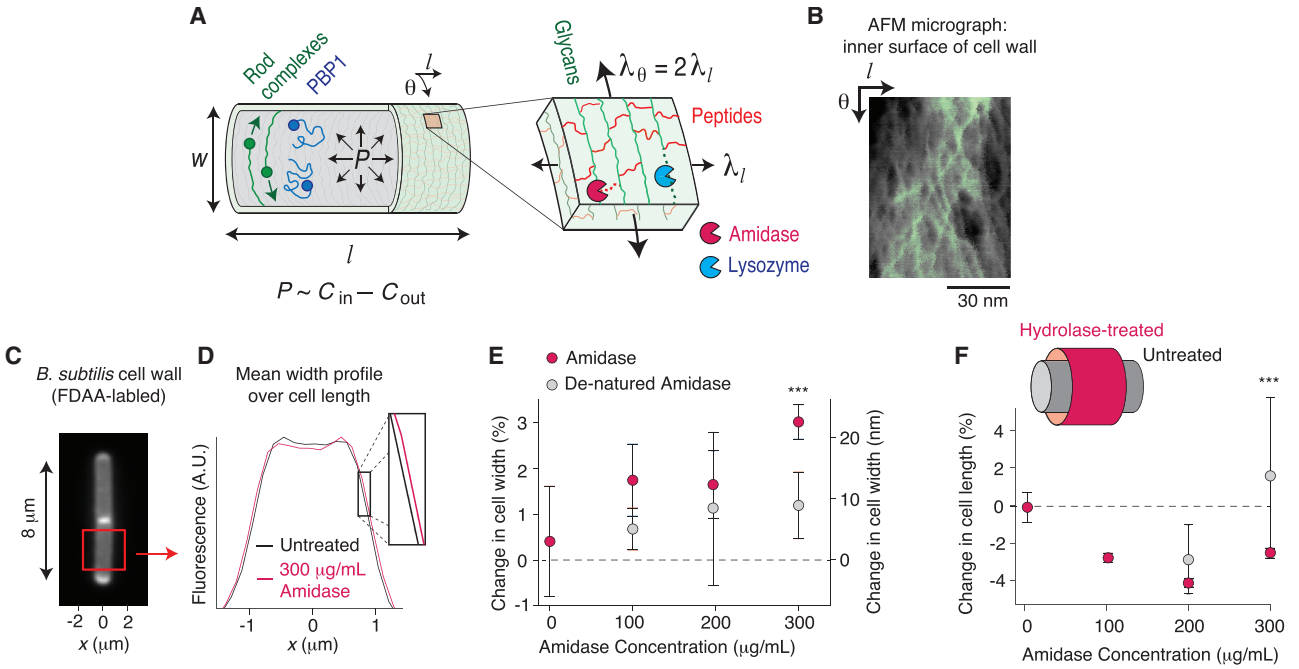

Figure 1. Exogenous peptide digestion causes cell widening

(A) Diagram of the Gram-positive cell wall, including its modes of synthesis and cell surface coordinate system (l,θ). P: turgor pressure. $\lambda_{l,\theta}$ are the longitudinal and circumferential surface tensions.

(B) Atomic force micrograph of the inner surface of the *B. subtilis* cell wall.[9] Raw micrograph courtesy of L. Pasquina-Lemonche.

(C) *B. subtilis* cell wall labeled with the fluorescent D-amino acid HADA.

(D) Fluorescent profile across the width of the labeled cell wall, averaged across cell length (red box in C) before and after 30 s of 300 μg/mL SPP1 amidase treatment.

(E) Mean change in cell width upon treatment with amidase and denatured amidase. Circumferential swelling upon denatured amidase could result from the microfluidic device and/or osmotic effects of the protein. Error bars indicate ± 1 SD. n = 15–50 cells across two technical replicates per data point.

(F) Mean change in cell length upon amidase treatment, controlling for cell growth. Error bars indicate ± 1 SD. n = 20–50 cells across two technical replicates per data point. Inset: illustration of the effect of hydrolases on cell wall dimensions. ***$p < 10^{-4}$, Student's two-sided t test (STSTT) comparing active and denatured measurements.

See also Figure S1.

amidase perfusion led to a small dose-dependent increase in width (Figure 1E). When controlling for cell growth, the enzyme had the opposite effect on cell length (Figure 1F). This is not consistent with longitudinally oriented peptides specifically being digested or with hydrolysis uniquely determining cell wall expansion. Perfusion of lysozyme, which digests the glycan moieties, led to the same qualitative effects (Figures S1B and S1C).

As an alternative method to measure the effect of hydrolysis on cell width, we perfused cells with an inhibitory concentration of vancomycin, which prevents cell wall synthesis without completely inhibiting hydrolysis,[14] leading eventually to lysis (Figure S1D). Vancomycin caused cell widening even before it reduced the elongation rate (Figure S1E). Together, these data indicate that peptidoglycan hydrolysis, when unbalanced by synthesis, leads to cell widening.

Considering these results, we hypothesized that cells exert a constrictive force on the cell wall to avoid gradual widening caused by the peptidoglycan hydrolysis required for cell growth. It was previously shown computationally that applying pre-stress to nascent glycan polymers could prevent pressure-driven widening,[15] but this mechanism was not tested, nor is there an obvious enzyme within the Rod complex that could exert pre-stress.

The cell wall is inflated to a non-linearity in its mechanical properties

The deformation of the cell wall upon peptidoglycan hydrolysis will depend on its mechanical properties. Atomic force microscopy is commonly used to probe these properties by measuring the deformation of the cell wall in response to indentation forces.[4] However, the largest forces that cells themselves generate are surface tensions within the cell wall that result from intracellular pressure (Figure 1A). Therefore, we measured cell wall mechanical properties by subjecting cells to a microfluidics-based "osmotic force-extension" assay that we previously established.[16] In this assay, cells are subjected to a series of osmotic shocks (Figure 2A), which cause acute changes in pressure. The pressure variations deform the cell wall (Figure 2B), and the dependence of this deformation (the longitudinal and circumferential strains, ε_l and ε_θ) on shock magnitude yields an empirical measurement of the anisotropic mechanical properties of the cell wall (Figures 2C, 2D, and S2).

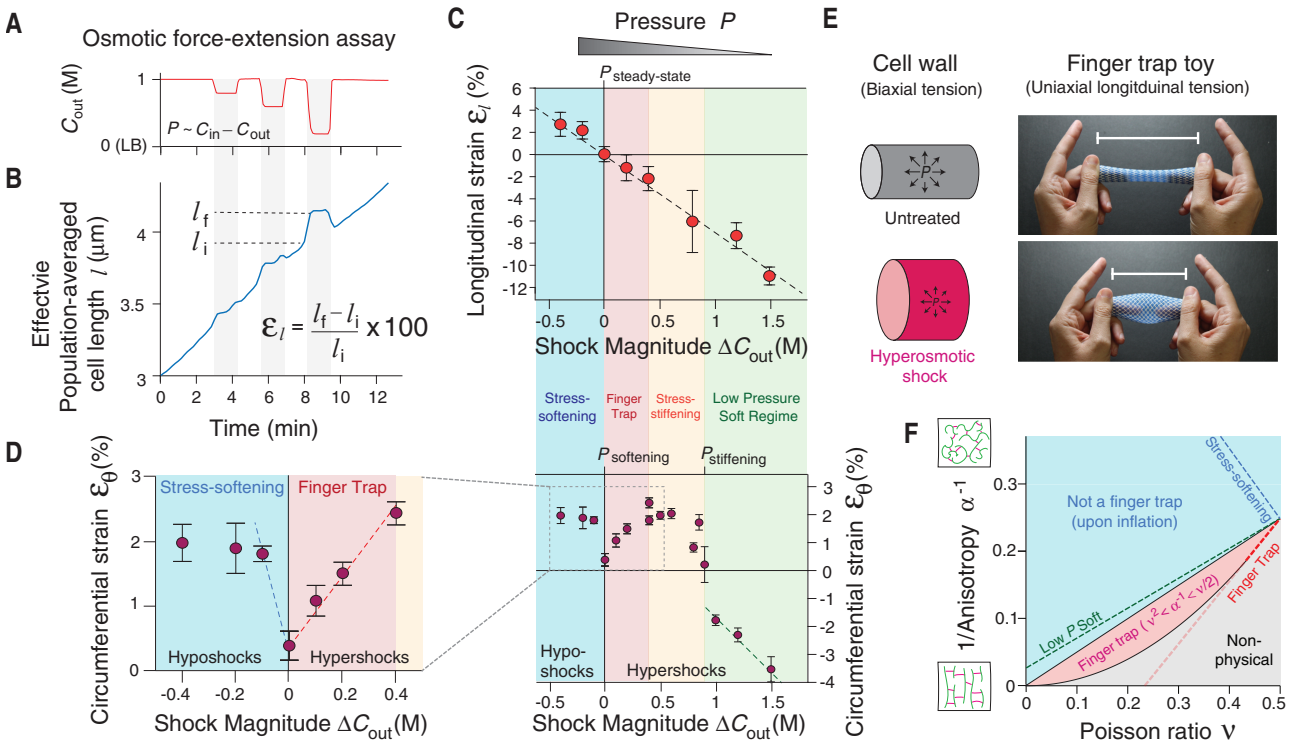

Figure 2. The cell wall exhibits anisotropic stress-stiffening and stress-softening

(A) Extracellular concentration of sorbitol, C_{out}, versus time during an osmotic force-extension experiment.

(B) Effective population-averaged cell length versus time during the osmotic force-extension experiment.

(C) Longitudinal strain versus shock magnitude across several osmotic-force-extension experiments. n = 20–60 cells across 1–3 replicate experiments per shock magnitude. Error bars: ±1 SEM. The dotted line is a linear regression.

(D) Circumferential strain versus shock magnitude across several osmotic-force-extension experiments. n = 74–174 cells across 1–2 replicate experiments per shock magnitude. Error bars: ±1 SEM. The dotted lines are linear regressions to the three linear regimes of mechanical behavior.

(E) Comparison of the deformation of the cell wall upon modest hyperosmotic shock to a finger-trap toy.

(F) The mechanical behavior of an inflated linear elastic cylindrical cell wall versus the anisotropy and Poisson ratio of the wall. The dotted lines are the behavior constrained by slopes of the regressions in (C) and (D).

See also Figures S2–S5.

As expected, hyperosmotic shocks, which decrease pressure, caused longitudinal contraction of the cell wall (negative longitudinal strain, $\varepsilon_l < 0$; Figure 2C), whereas hypoosmotic shocks, which increase pressure, caused longitudinal stretching ($\varepsilon_l > 0$). Moreover, longitudinal strain was inversely proportional to shock magnitude and reversible (Figures 2B and 2C), meaning that the cell wall is linearly elastic in this dimension.

To measure deformation in cell width, we combined our osmotic force-extension assay with super-resolution measurements of circumferential strain. As for the longitudinal direction, small 100 mM hypoosmotic shocks caused circumferential stretching of the cell wall (Figures 2C and 2D). Larger shocks did not cause further circumferential stretching even though they did cause additional longitudinal stretching. Like hypoosmotic shocks, modest hyperosmotic shocks also caused circumferential stretching even though they reduced pressure (Figure 2C). That is, small decreases in pressure had the opposite effects on cell length and width, similar to the effect of exogenous peptidoglycan hydrolysis (Figures 1E, 1F, S1B, and S1C). This was reminiscent of a finger-trap toy in which longitudinal compression causes circumferential stretching due to mechanical coupling between the two axes of deformation (Figure 2E). However, we did not expect this behavior for the cell wall since the tension induced in it by turgor pressure is not uniaxial, as it is for the toy: reducing pressure decreases circumferential tension approximately twice as much as longitudinal tension due to the rod-shaped geometry of the cell[12] (STAR Methods). Furthermore, our previous experiments with *E. coli* did not exhibit this behavior even though its cell wall is also anisotropic.[17]

It was previously reported that small hyperosmotic shocks cause thinning of *B. subtilis* cells[14] as measured with phase microscopy, ostensibly contradicting our results. However, using our method, we also observed thinning upon hyperosmotic shock when we used the plasma membrane to measure cell width (Figure S3A), revealing that the cell wall and plasma membrane deform independently. To support this finding, we used transmission electron microscopy to image the cell envelope of chemically fixed cells before and after hyperosmotic shock (Figure S3B). In unshocked cells, the plasma membrane appeared flush with the cell wall, whereas after hyperosmotic shock, there was a gap between the membrane and wall,

explaining how these structures could deform in opposite directions. A similar gap between the wall and membrane was observed previously in cryo-fixed cells.[18]

The cell wall exhibited linear finger-trap deformation for hyperosmotic shocks up to ΔC_{out} = 400 mM (Figure 2C); however, we observed highly non-linear behavior outside of this range. First, for hyperosmotic shocks between 400 and 800 mM, the circumferential strain plateaued. At ΔC_{out} ≈800 mM, we observed a sharp decrease in circumferential strain, whereas for larger shocks it decreased linearly. Second, since small hypoosmotic shocks caused circumferential swelling of the cell wall, the cell wall is inflated precisely to a sharp non-linearity in the mechanical properties of the cell wall during steady-state growth.

The cell wall exhibits anisotropic stress-stiffening and -softening

It was instructive to use linear elasticity theory to interpret the dependences of the principal strains on shock magnitude in the different empirical pressure regimes—this is the two-dimensional equivalent of performing a local linear fit of a non-linear one-dimensional force-extension curve to obtain an effective stiffness. For an anisotropic two-dimensional material, linear elasticity can be expressed (STAR Methods):

$$\begin{pmatrix} \varepsilon_l \\ \varepsilon_\theta \end{pmatrix} = \frac{1}{E_l} \frac{1}{\alpha(\alpha^{-1} - \nu^2)} \begin{pmatrix} 1 & -\nu \\ -\nu & \alpha^{-1} \end{pmatrix} \begin{pmatrix} \lambda_l \\ \lambda_\theta \end{pmatrix}, \quad \text{(Equation 1)}$$

where E_l is the longitudinal elastic modulus, $\alpha = E_\theta/E_l$ is the mechanical anisotropy (ratio of the principal elastic moduli), and ν is a Poisson ratio (generalized to the case of material anisotropy). The surface tensions, $\lambda_l = PR/2$ and $\lambda_\theta = PR$, balance pressure.[12] Imposing the condition that ε_l and ε_θ have opposite signs when pressure is altered reveals that the cell wall deforms as a finger trap if $\alpha^{-1} < \nu/2$, that is, if it is sufficiently anisotropic (Figure 2F; STAR Methods).

Although the empirical dependence of the strains on shock magnitude (Figures 2C and 2D) does not uniquely define α and ν, it constrains them to a line in the two-dimensional (α^{-1}, ν) parameter space (Figure 2F). For the pressure regime resulting in finger-trap deformation, this analysis demonstrated that the Poisson ratio of the cell wall is between $0.45 < \nu < 0.5$ and that α is as high as is physically possible within that range, assuming there is no other source of tension than pressure.

A similar analysis for the mechanical behavior in the "low-pressure regime" (ΔC_{out} > 800 mM) demonstrated that the cell wall has a lower value of anisotropy than in the finger-trap regime (Figure 2F). Since the linear dependence of the longitudinal strain on shock magnitude is independent of pressure (Figure 2C), this means that the transition from the low-pressure regime to the finger-trap regime reflects anisotropic stress stiffening[4] exclusively in the circumferential direction.

Similarly, the observation that cells do not behave as a finger trap for hypoosmotic shocks means that the wall is effectively softening (exclusively) in the circumferential direction when pressure is increased beyond its steady-state value (Figure 2F). Therefore, the cell wall undergoes anisotropic stress-stiffening and stress-softening at different values of pressure (Figure 2C).

The molecular basis for stress-stiffening and -softening is beyond the scope of this study, but we suggest a qualitative working model for this behavior (Figure S4). First, at low pressures, the cell wall is relatively soft in the circumferential direction because the glycan moieties are not fully extended (circumferential strain is low). In this soft state, the glycans can be thought of as circumferential slack. Therefore, increasing pressure causes the cell wall to stretch circumferentially. However, when the cell wall is sufficiently inflated, the circumferentially oriented glycans undergo conventional stress-stiffening (they become taut), which increases anisotropy and leads to finger-trap deformation. In this state, as pressure increases, the cell wall contracts circumferentially, decreasing cell width. Finally, when pressure exceeds a critical value, contraction causes glycans to exit their taut state, leading to circumferential softening of the cell wall and loss of finger-trap deformation, and further increase of pressure therefore causes cell widening. In this picture, stress-softening is essentially "strain-stiffening" in reverse. However, since circumferential strain depends non-monotonically on pressure, circumferential stiffness and anisotropy must also depend on longitudinal strain. For example, there are values of pressure in the stress-stiffening, finger-trap, and stress-softening regimes that yield 1% circumferential strain but correspond to different values of anisotropy (Figure 2C)—the difference between these three states is the longitudinal strain.

Finger-trap deformation is correlated with cell-width control

Because finger-trap deformation corresponds to constriction of cell width upon elongation, our results raised the possibility that this behavior was required to avoid runaway widening during cell growth. To explore this hypothesis theoretically, we constructed a simple physical model for the irreversible mechanical expansion of a linear elastic, layered cell wall that accounts for dynamics of cell length and width (Figure 3A). The molecular-scale spatial relationship of peptidoglycan synthesis and hydrolysis during cell growth is unknown, but since rod complexes are membrane-bound, it is believed that synthesis of non-load-bearing peptidoglycan occurs adjacent to the membrane, whereas the hydrolysis of load-bearing peptidoglycan required for cell growth occurs further from the membrane.[19] We therefore considered a model in which layers of anisotropic peptidoglycan are added to the inner face of the cell wall at a constant rate, and they are removed at the same rate from the outer face via hydrolysis (STAR Methods). Since the cell wall is under tension, removal of load-bearing peptidoglycan from the outer face dissipates energy and causes irreversible deformation, or growth, of the cell wall.

When we solved this model computationally across α and ν, we found that the region of parameter space in which cells thin during growth was identical to the region where the cell wall behaves as a finger trap, mechanically (compare Figure 3B to 2F). Equivalently, cells widen during simulations of cell growth for parameter values that do not yield finger-trap deformation. The reason for the correspondence between the elastic behavior and growth dynamics is simple: when load-bearing peptidoglycan is removed from the cell wall, the wall must deform to balance pressure, and since we analyzed a linear model, the cell wall deforms as a finger trap regardless of the strain distribution across the normal direction (Figure 3A). Importantly, any model in which the cell wall is linear elastic will behave equivalently unless mechanical energy is dissipated by specifically relieving

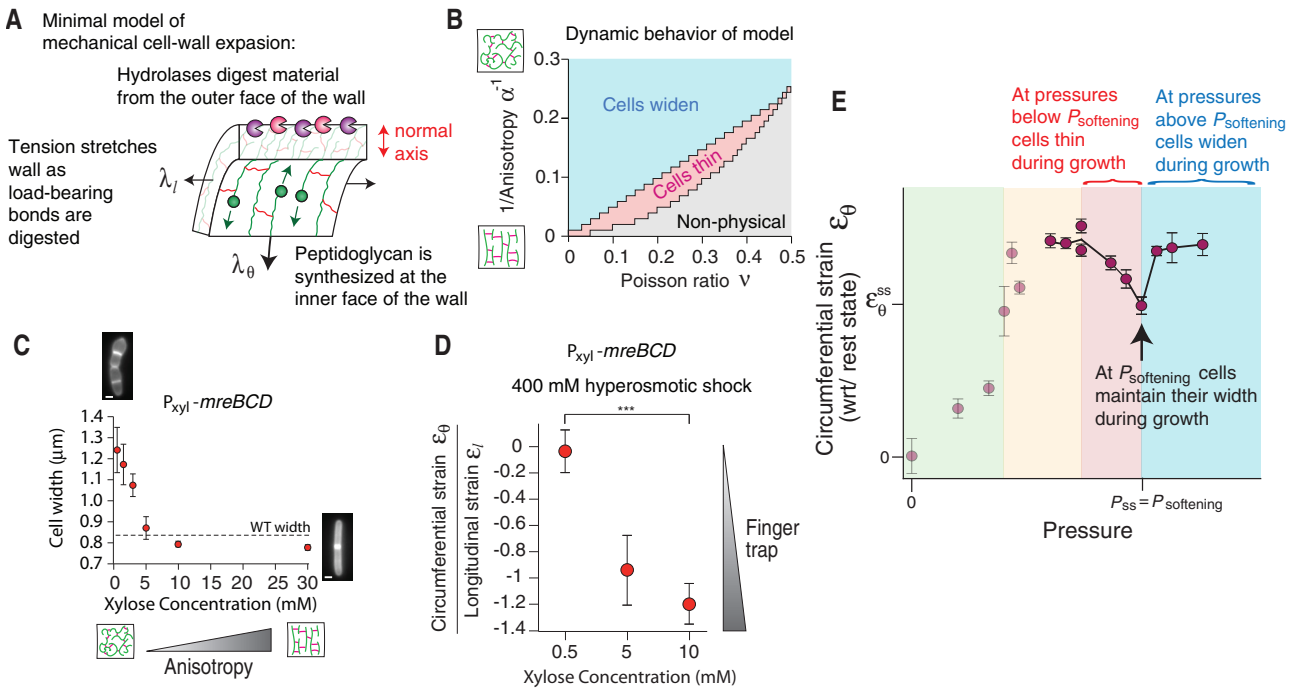

Figure 3. Finger-trap mechanics are correlated with cell-width control

(A) Diagram of the components of the theoretical linear elastic model for cell growth.

(B) Dynamic behavior of the model versus the anisotropy and Poisson ratio.

(C) Cell width versus induction of *mreBCD*. n = 22–57 cells across 1 replicate per induction level. Error bars: ±1 SD.

(D) Ratio of circumferential strain and longitudinal strain upon 400 mM hyperosmotic shock for three induction levels of *mreBCD*. Values were calculated from n = 26–90 cells across 1–3 replicate experiments (circumferential strain) and n = 60–78 cells across 1 replicate experiment (longitudinal strain) per induction level. Error was propagated from the SEM for each respective measurement. ***$p < 10^{-4}$, STSTT compared with 5 mM measurement.

(E) Graphical description of how the dependence between circumferential strain and pressure determines cell width dynamics. The data are the same as shown in Figure 2D.

stress in the longitudinal direction, which is a generalization of our model and would only expand the region of the parameter space leading to finger-trap deformation and thinning during growth.

Therefore, according to this model, the cell will maintain its width if its cell wall has mechanical properties that are on the boundary between the finger-trap and non-finger-trap regions of parameter space (Figure 3E). Our data demonstrate that cells achieve this by inflating themselves, precisely, to a non-linearity between pressure regimes that exhibit finger-trap and non-finger-trap behavior, respectively.

We reasoned that if the non-linearity, which implicitly requires finger-trap deformation upon pressure reduction, enables cell growth at a constant width, then the existence of finger-trap deformation would be correlated with rod-shaped growth. To test this, we perturbed cell shape by genetically manipulating the structural anisotropy of the cell wall and simultaneously measured the effect of these perturbations on circumferential deformation during hyperosmotic shock. To alter cell wall anisotropy, we titrated the expression of the *mreBCD* operon, which encodes several Rod-complex components, via xylose induction.[20] When biosynthetic flux through Rod complexes is reduced, the balance is accommodated by PBP1, a non-essential enzyme that synthesizes peptidoglycan isotropically (Figure 1A). Therefore, when the relative expression of the Rod complex is reduced below wild-type levels, cell width increases (Figure 3D). At very low levels (xylose concentrations < 1 mM), cells lose rod shape and grow semi-amorphously.

As our model predicted, for Rod-complex expression high enough to generate rods, 400 mM hyperosmotic shock led to circumferential stretching and longitudinal contraction, leading to negative values of $\varepsilon_\theta/\varepsilon_l$ (Figure 3E). Conversely, for Rod-complex expression that led to amorphous growth (0.5 mM xylose), the cell wall no longer stretched circumferentially upon hyperosmotic shock. That is, there was a strong correlation between whether the cell maintained a rod shape and whether the cell exhibited finger-trap deformation upon hyperosmotic shock. For the expression level that resulted in amorphous growth, the cell wall was still highly anisotropic ($\alpha > 4$), demonstrating that the non-linearity associated with finger-trap deformation, rather than anisotropy alone, is the key factor underlying cell growth at constant width.

Pressure-induced wall softening confers width homeostasis

Our analysis explained how cells maintain a constant cell width by inflating themselves precisely to the stress-softening non-linear transition, which is the critical pressure in between pressure regimes that cause widening and thinning, respectively

(Figure 3E). However, our model also predicted that deviations from this pressure would lead to either constitutive widening or thinning. How do cells achieve width homeostasis? We posited that the non-linear transition could confer an intrinsic mechanism for width homeostasis if there was feedback between cell width, pressure, and/or the critical pressure at which the transition occurs. For example, for cells that are wider than their steady-state width but are dynamically thinning (Figure 4A), we predicted that the cell wall would be inflated to the finger-trap regime and that pressure would converge with the critical pressure of the non-linear transition as width approached its steady-state value.

To test this, we cultured cells to steady-state growth at low Rod-complex expression, acutely induced high Rod-complex expression (Figure 4A), and then performed circumferential osmotic-force-extension experiments before, during, and after relaxation to steady state. As for wild-type bacteria, both hypo- and hyperosmotic shocks caused circumferential swelling of the cell wall for cells grown to steady state at low, medium, and high Rod-complex expression (Figures 4B–4D). However, hypoosmotic shocks up to 600 mM caused thinning of cell wall width for cells that were actively thinning (Figure 4D). In other words, during cell thinning, the cell wall was inflated to the finger-trap regime, not the non-linearity. The validation of this non-intuitive prediction strongly supports our model that bacteria exploit the non-linear mechanical properties of their cell wall to homeostatically control cell width. Further supporting this model, the circumferential stretching we observed immediately after modest hyperosmotic shock of wild-type cells was transient (Figure S5): this is expected if deflation of the cell wall into the finger-trap regime subsequently causes cell thinning, although osmoregulation[21] will also influence these dynamics.

After acute de-induction of Rod-complex expression, there was a long, variable lag time before cells began to grow and widen, which prevented us from testing whether the cell wall was inflated to the stress-softening regime during widening. However, our observation that the cell wall is in the finger-trap regime during thinning but not during steady-state growth suggested that turgor pressure and/or the critical pressure of the non-linear transition are variable during width adaptation. Since finger-trap-mediated cell thinning occurs when turgor pressure is lower than the critical stress-softening pressure, we considered two possibilities for the mechanism of cell width homeostasis after acute Rod complex induction: (1) that thinning increases pressure until it equals the critical stress-softening pressure, which then leads to widening, or (2) that thinning leads to a decrease of the critical pressure of the stress-softening transition until it equals the actual pressure, leading to widening. Either of these processes would provide a negative-feedback loop that regulates cell width.

To measure pressure, we performed our longitudinal osmotic-force-extension assay (Figure 2C), and in a second experiment we lysed cells and measured length contraction upon loss of turgor pressure. We thus quantified the magnitude of hyperosmotic shock that caused contraction of the cell wall to the same length as cell lysis, which gives an empirical measurement of turgor pressure in units of osmolarity (Figure 4E).

Contrary to our initial expectations, we found that turgor pressure was inversely dependent on Rod-complex expression (Figure 4F). This corresponded to a positive correlation between pressure and cell width during steady-state growth. Since, at steady state, cells are inflated to the stress-softening non-linearity regardless of Rod-complex expression level (Figures 4B–4D), these measurements led us to conclude that the critical stress-softening pressure is dynamic during width adaptation.

Despite the correlation between pressure and cell width during steady-state growth, upon acute induction of Rod-complex expression, pressure equilibrated to its low, steady-state value rapidly, while cells were still thinning ($\leq$15 min; Figure 4F), and therefore before the critical pressure of the non-linearity had been established at the new low pressure (Figure 4D). This implied that pressure is directly dependent on the specific molecular architecture of the cell wall (determined by the balance of Rod-complex and PBP1 expression) rather than directly on width.

The migration of the non-linear transition to lower pressures as cells thin led us to a model for cell width homeostasis that incorporates molecular and mechanical signals (Figures 4G and 4H). According to this model, if cells are wider than their target steady-state value, then their pressure is lower than the critical pressure of the stress-softening non-linearity, the cell wall is in the finger-trap regime, and cells thin dynamically during growth. As cells thin, the critical pressure (a mechanical property of the cell wall) decreases until it reaches the actual pressure, and further thinning would position the cell wall in the stress-softening regime, which would cause them to widen, completing the negative feedback. Conversely, if cells are thinner than their steady-state width, then their cell wall is in the stress-softening regime, and they widen during cell growth until the critical pressure increases until the actual pressure.

Finger-trap deformation is exhibited by other Gram-positive rod-shaped bacteria and plants

We explored the generality of this mechanism of cell-width control by testing for finger-trap deformation across other organisms. Like *B. subtilis*, the Gram-positive rod-shaped bacterium *Listeria seeligeri* also exhibited finger-trap deformation upon hyperosmotic shock (Figure 5A). Conversely, *Corynebacterium glutamicum*, another rod-shaped Gram-positive bacterium, did not exhibit finger-trap deformation. However, unlike *B. subtilis* and *L. selegerii*, *C. glutamicum* elongates via polar growth: for this mode of growth, cell width must be maintained through control of the size of the polar growth zone, and therefore *C. glutamicum* would have no use for the mechanism we described here. Previous measurements of *E. coli* did not exhibit finger-trap deformation,[17] a result we confirmed here. This means that neither finger-trap deformation nor the non-linearity are inevitable properties of anisotropic peptidoglycan and that Gram-negative bacteria use another mechanism to control width in spite of turgor pressure. Since pressure is much lower in these species,[4] anisotropy in peptidoglycan insertion or pre-stretching of glycans[15] may play a greater role than in Gram-positive bacteria. Finally, we discovered that the roots of *Arabidopsis thaliana* plants, which are multicellular elliptic cylindrical tissues that, like rod-shaped bacteria, grow along their length and must maintain their width, are also inflated precisely to a non-linearity equivalent to the one we identified in *B. subtilis* (Figures 5B, 5C, and S6), which may represent a remarkable example of convergent mechanobiology.

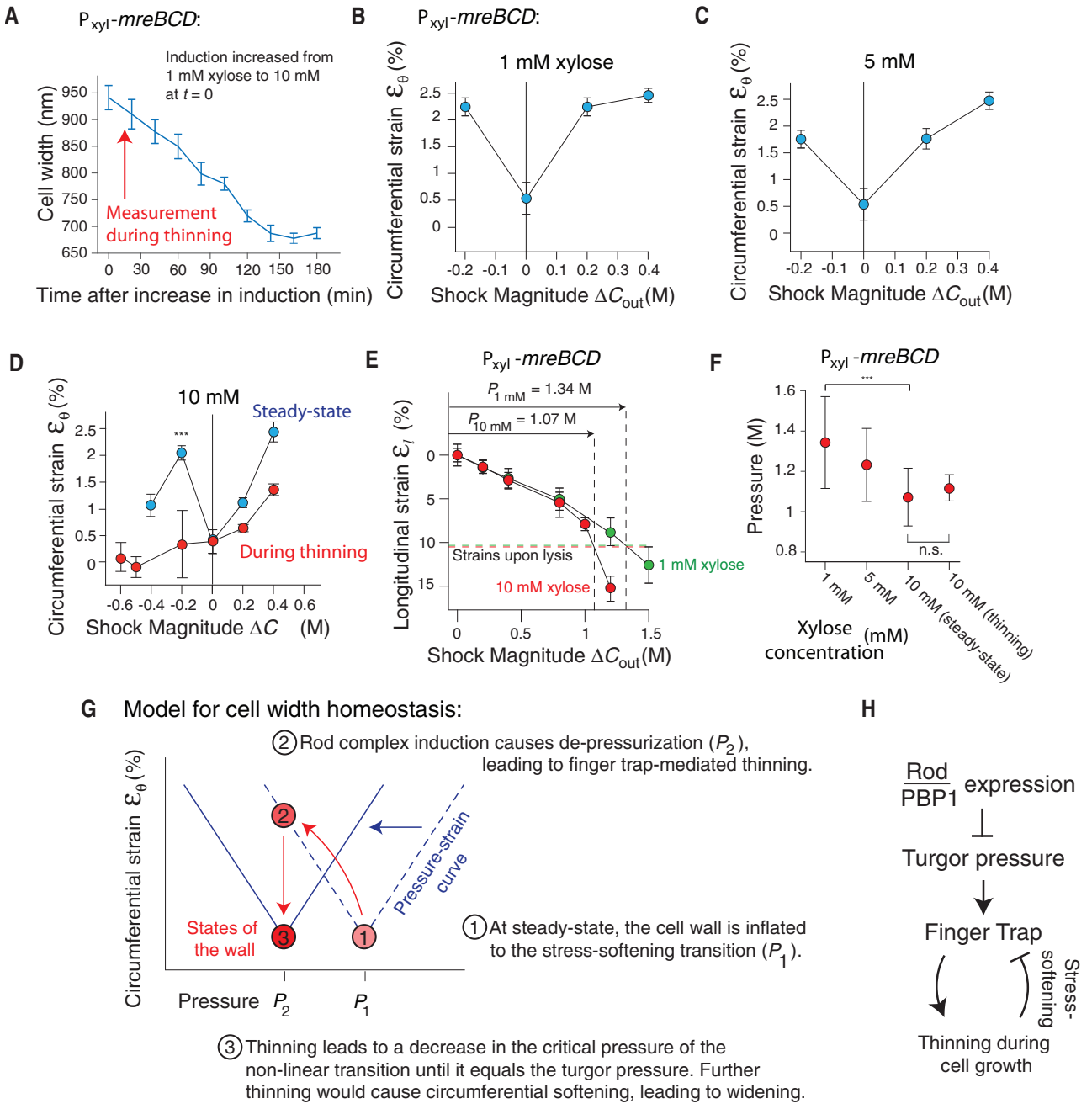

Figure 4. Strain-softening confers cell width homeostasis

(A) Cell width versus time after acute induction of *mreBCD*. Cells were grown to exponential phase in 1 mM xylose, and then xylose concentration was increased to 10 mM. n = 20 cells across 1 experiment for each time point.

(B–D) Circumferential strain versus shock magnitude at 1, 5, and 10 mM xylose induction of P_{xyl}-*mreBCB*. n = 30–50 cells across 1–3 replicate experiments per shock magnitude. Error bars: ±1 SEM.

(E) Assay to measure turgor pressure by measuring the magnitude of hyperosmotic shock that causes the cell wall to contract to its rest length. n = 60–175 cells across 1–2 replicate experiments per shock magnitude. n = 73–90 cells across 2 replicate experiments for each lysis strain measurement. ***$p < 10^{-4}$, STSTT compared with 1 mM measurement.

(F) Mean turgor pressure versus induction of P_{xyl}-*mreBCB*. Error was propagated from that of the lysis strain and regression of the osmotic force-extension (STAR Methods).

(G and H) Qualitative negative-feedback model of cell width homeostasis based on finger-trap mechanics and stress-softening.

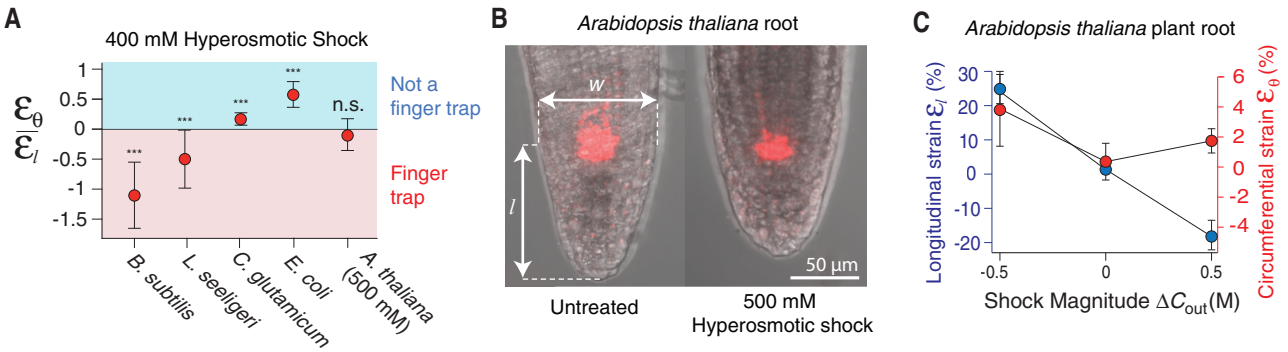

Figure 5. Plant roots are also inflated to a stress-softening non-linearity

(A) Ratio of circumferential strain and longitudinal strain upon 400 mM hyperosmotic shock for wild-type *B. subtilis*, *L. seeligeri*, *C. glutamicum*, *E. coli*, and *A. thaliana* roots. *B. subtilis* statistics are the same as in Figures 2C and 2D. For *L.s.* $n = 20$ cells across one experiment. *C.g.*: $n = 20$ cells across 1 experiment for circumferential strain and $n = 306$ across 1 experiment for longitudinal strain. For *E.c.*: $n = 22$–37 cells across two experimental replicates for circumferential strain, $n = 238$ cells across 3 experimental replicates for longitudinal strain. For *A.t.*: $n = 6$ biological replicates (roots). $^{***}p < 10^{-4}$, STSTT compared with zero. Error bars were propagated from ± 1 SEM.

(B) Representative micrographs of an *Arabidopsis thaliana* root before and after 500 mM hyperosmotic shock. The roots are aligned by their quiescent center, which expresses mCherry and was used as a fiducial marker to calculate strains.

(C) Longitudinal and circumferential strain versus shock magnitude for *A. thaliana* plant roots. n = 13, 6, and 7 roots for untreated, hyperosmotic shock, and hypoosmotic shock experiments. Error bars: ±1 SD.

DISCUSSION

Transduction of forces within mammalian cells is mediated by molecular mechanosensors[22] that elicit biochemical and genetic responses, which, in turn, manipulate forces within the cell. For example, when force is applied to branched actin networks, they rapidly increase the amount of force they can sustain through structural alterations, a process that is hardwired into the biochemistry of actin-binding proteins.[23] Like actin, we found that the Gram-positive bacterial cell wall is a "smart material" that internally senses and responds to forces. In this paradigm, negative-feedback regulation of cell width is embedded the non-linear properties of the wall.

One important question that is motivated by our model is the mechanistic basis underlying the inverse correlation between Rod-complex expression and turgor pressure (Figure 4E). In concurrent work,[24] we identified a molecular mechanism by which *B. subtilis* directly senses cell wall microstructure and relays this information to osmoregulation systems via cyclic-di-AMP signaling, which could explain this correlation. Consistent with this hypothesis, we found that when pressure was modulated by altering cyclic-di-AMP levels, cell width was correlated with pressure, as our model predicts.

A second open question is the specific mechanism by which the critical pressure of the non-linear transition depends on cell width. We hypothesize that a key variable missing from our model is the surface area-to-mass ratio, which determines the metabolic flux through the peptidoglycan biosynthesis pathway.[14] For example, the critical pressure could depend on the quantitative ratio between this flux and the rate of peptidoglycan hydrolysis. Combined with our model, such a mechanism would provide quantitative scaling relationships that predict how cell width depends on environmental variables, including nutrients and osmotic pressure.

The two-dimensional mechanical model that we used to analyze our data (Equation 1) implicitly ignores mechanical stress in the direction normal to the cell wall. Normal stress will be much smaller than surface tensions since the cell wall is relatively thin compared with the cell[12] but could still perform physiological functions during cell growth. Importantly, generalizing our model to include normal stress would only expand the space of mechanical behavior, including the region yielding finger-trap deformation (Figure 2F); therefore, the model we used is the most conservative one that explains our data. However, we observed preliminary evidence of normal stress from our transmission electron microscopy data (Figures S3B–S3D). Specifically, we found that hyperosmotic shock not only caused detachment of the cell wall from the plasma membrane but also caused slight thinning of the cell wall (on time scales much faster than hydrolysis could be expected to do so). These data need to be validated further since the fixation protocol prior to imaging causes lysis and deformation of the cells, but if confirmed, this would mean that the wall is stretched in the normal direction during steady-state growth. This would contribute to circumferential constriction via mechanical coupling of the normal and circumferential directions and could play a role in supporting the molecular physiology of cell growth near the membrane. The origin of such a tensile normal stress is not obvious.

The non-linearity corresponding to stress-softening as well as the migration of the critical pressure of the non-linearity during width adaptation were unforeseen mechanical behaviors. Stress-stiffening (or strain-stiffening) of polymer networks is a more familiar phenomenon that occurs, for example, due to stretching of polymers beyond their soft "entropic" regime.[25] In the present case, softening and stiffening may be two sides of the same coin since within the finger-trap regime, stress reduces circumferential strain. However, it is unlikely that the stress-softening non-linearity can be explained with existing paradigms given the narrow range of strain over which it occurs. Finally, for the Gram-positive cell wall, stress-stiffening is likely to be a requirement for the existence of finger-trap behavior (and, in turn, stress-softening) due to geometric constraints. Specifically, since

peptidoglycan is synthesized at or near the plasma membrane, it must stretch circumferentially as it is advected through the wall during cell growth.[19] However, if peptidoglycan were in the finger-trap regime when it is synthesized, it would only contract during growth. Therefore, stress-stiffening and -softening are probably both required for width homeostasis, underscoring the exquisite, adaptive mechanical properties of the cell wall.

At this point, we can only speculate as to the detailed molecular basis for stress-stiffening, stress-softening, or migration of the non-linearity, which will depend on the complex but poorly understood interactions between peptidoglycan synthases, hydrolases, and the microstructure of the cell wall. This will be a major challenge since, after all, even linear elasticity is a phenomenological model. The cell wall's extraordinary non-linear mechanical properties, however, are clearly functional for the cell. Ultimately, biological mechanism is physical phenomenology, and a deeper materials science understanding of the mechanics we have described will be an exciting direction for future research.

RESOURCE AVAILABILITY

Lead contact

Requests for further information and resources should be directed to and will be fulfilled by the lead contact, Enrique Rojas (rojas@nyu.edu).

Materials availability

No new bacterial strains or reagents were generated during this study.

Data and code availability

- All data reported in this paper will be shared by the lead contact upon request.
- All original code has been deposited at the Rojas Lab GitHub repository and is publicly available at https://github.com/TheRojasLab/Bardetti2026.
- Any additional information required to reanalyze the data reported in this paper is available from the lead contact upon request.

ACKNOWLEDGMENTS

E.R.R. and P.B. were supported by NIH R35GM143057. F.B. was supported by NSF CAREER 2047404. The NYULH Microscopy Lab was partially supported by NIH/NCI P30CA016087. We thank Ethan Garner, Carlos São-José, Alex Meeske, Harold Erickson, and members of Tania Lupoli's Lab for strains, plasmids, technical assistance, and insightful discussions. The AFM micrograph in Figure 1A was taken by Laia Pasquina-Lemonche. TEM was performed by Alice Liang, Jason Yin, and Jason Liang of the NYULH Microscopy Lab.

AUTHOR CONTRIBUTIONS

Conceptualization, P.B. and E.R.R.; data curation, P.B.; formal analysis, E.R.R. and F.B.; funding acquisition, E.R.R.; investigation, P.B. and D.F.; methodology, P.B. and E.R.R.; project administration, E.R.R.; software, P.B.; supervision, E.R.R.; validation, P.B.; visualization, P.B. and E.R.R.; writing – original draft, P.B. and E.R.R.; writing – review & editing, P.B. and E.R.R.

DECLARATION OF INTERESTS

The authors declare no competing interests.

STAR★METHODS

Detailed methods are provided in the online version of this paper and include the following:

- KEY RESOURCES TABLE
- EXPERIMENTAL MODEL AND STUDY PARTICIPANT DETAILS
  - *Bacillus subtilis* PY79
  - *B. subtilis* bMD545
  - *B. subtilis* bZB112
  - Corynebacterium glutamicum
  - Escherichia coli MG1655
  - Listeria seeligeri
  - Arabidopsis thaliana
  - Culture Conditions
- METHOD DETAILS
  - Light microscopy
  - Spp1 endolysin purification
  - Osmotic force-extension assays
  - Super-resolution measurement of single-cell width deformation
  - Hydrolysis assay
  - Derivation of Equation 1 and theoretical phase space
  - Cell lysis assay
  - Pressure measurements
  - Mathematical model of cell morphogenesis
  - Transmission electron microscopy
  - Osmotic shocks on Arabidopsis roots
- QUANTIFICATION AND STATISTICAL ANALYSIS

SUPPLEMENTAL INFORMATION

Supplemental information can be found online at https://doi.org/10.1016/j.cub.2026.01.043.

Received: April 15, 2025
Revised: December 2, 2025
Accepted: January 19, 2026
Published: February 16, 2026

REFERENCES

1. Typas, A., Banzhaf, M., Gross, C.A., and Vollmer, W. (2011). From the regulation of peptidoglycan synthesis to bacterial growth and morphology. Nat. Rev. Microbiol. *10*, 123–136. https://doi.org/10.1038/nrmicro2677.
2. Vollmer, W., Joris, B., Charlier, P., and Foster, S. (2008). Bacterial peptidoglycan (murein) hydrolases. FEMS Microbiol. Rev. *32*, 259–286. https://doi.org/10.1111/j.1574-6976.2007.00099.x.
3. Rojas, E.R., Huang, K.C., and Theriot, J.A. (2017). Homeostatic cell growth is accomplished mechanically through membrane tension inhibition of cell-wall synthesis. Cell Syst. *5*, 578–590.e6. https://doi.org/10.1016/j.cels.2017.11.005.
4. Deng, Y., Sun, M., and Shaevitz, J.W. (2011). Direct measurement of cell wall stress stiffening and turgor pressure in live bacterial cells. Phys. Rev. Lett. *107*, 158101. https://doi.org/10.1103/PhysRevLett.107.158101.
5. Whatmore, A.M., and Reed, R.H. (1990). Determination of turgor pressure in Bacillus subtilis: a possible role for K+ in turgor regulation. Microbiology *136*, 2521–2526. https://doi.org/10.1099/00221287-136-12-2521.
6. Garner, E.C. (2021). Toward a mechanistic understanding of bacterial rod shape formation and regulation. Annu. Rev. Cell Dev. Biol. *37*, 1–21. https://doi.org/10.1146/annurev-cellbio-010521-010834.
7. Garner, E.C., Bernard, R., Wang, W., Zhuang, X., Rudner, D.Z., and Mitchison, T. (2011). Coupled, circumferential motions of the cell wall synthesis machinery and MreB filaments in B. subtilis. Science *333*, 222–225. https://doi.org/10.1126/science.1203285.
8. Domínguez-Escobar, J., Chastanet, A., Crevenna, A.H., Fromion, V., Wedlich-Söldner, R., and Carballido-López, R. (2011). Processive movement of MreB-associated cell wall biosynthetic complexes in bacteria. Science *333*, 225–228. https://doi.org/10.1126/science.1203466.
9. Pasquina-Lemonche, L., Burns, J., Turner, R.D., Kumar, S., Tank, R., Mullin, N., Wilson, J.S., Chakrabarti, B., Bullough, P.A., Foster, S.J.,

et al. (2020). The architecture of the Gram-positive bacterial cell wall. Nature *582*, 294–297. https://doi.org/10.1038/s41586-020-2236-6.

10. Auer, G.K., and Weibel, D.B. (2017). Bacterial cell mechanics. Biochemistry *56*, 3710–3724. https://doi.org/10.1021/acs.biochem.7b00346.
11. Vollmer, W., and Bertsche, U. (2008). Murein (peptidoglycan) structure, architecture and biosynthesis in Escherichia coli. Biochim. Biophys. Acta *1778*, 1714–1734. https://doi.org/10.1016/j.bbamem.2007.06.007.
12. Love, A.E.H. (1897). Theoretical Mechanics: An Introductory Treatise on the Principles of Dynamics with Applications and Numerous Examples (University Press).
13. Fernandes, S., and São-José, C. (2016). More than a hole: the holin lethal function may be required to fully sensitize bacteria to the lytic action of canonical endolysins. Mol. Microbiol. *102*, 92–106. https://doi.org/10.1111/mmi.13448.
14. Kitahara, Y., Oldewurtel, E.R., Wilson, S., Sun, Y., Altabe, S., de Mendoza, D., Garner, E.C., and van Teeffelen, S. (2022). The role of cell-envelope synthesis for envelope growth and cytoplasmic density in Bacillus subtilis. PNAS Nexus *1*, pgac134. https://doi.org/10.1093/pnasnexus/pgac134.
15. Furchtgott, L., Wingreen, N.S., and Huang, K.C. (2011). Mechanisms for maintaining cell-shape in rod-shaped Gram-negative bacteria. Biophys. J. *100*, 514a.
16. Fitzmaurice, D.R., Amador, A., Starr, T., Hocky, G.M., and Rojas, E.R. (2025). β-barrel proteins dictate the effect of core oligosaccharide composition on outer membrane mechanics. Biophys. J. *124*, 765–777. https://doi.org/10.1016/j.bpj.2025.01.017.
17. Rojas, E., Theriot, J.A., and Huang, K.C. (2014). Response of Escherichia coli growth rate to osmotic shock. Proc. Natl. Acad. Sci. USA *111*, 7807–7812. https://doi.org/10.1073/pnas.1402591111.
18. Matias, V.R.F., and Beveridge, T.J. (2005). Cryo-electron microscopy reveals native polymeric cell wall structure in Bacillus subtilis 168 and the existence of a periplasmic space. Mol. Microbiol. *56*, 240–251. https://doi.org/10.1111/j.1365-2958.2005.04535.x.
19. Koch, A.L., and Doyle, R.J. (1985). Inside-to-outside growth and turnover of the wall of gram-positive rods. J. Theor. Biol. *117*, 137–157. https://doi.org/10.1016/S0022-5193(85)80169-7.
20. Dion, M.F., Kapoor, M., Sun, Y., Wilson, S., Ryan, J., Vigouroux, A., van Teeffelen, S., Oldenbourg, R., and Garner, E.C. (2019). Bacillus subtilis cell diameter is determined by the opposing actions of two distinct cell wall synthetic systems. Nat. Microbiol. *4*, 1294–1305. https://doi.org/10.1038/s41564-019-0439-0.
21. Whatmore, A.M., Chudek, J.A., and Reed, R.H. (1990). The effects of osmotic upshock on the intracellular solute pools of Bacillus subtilis. J. Gen. Microbiol. *136*, 2527–2535. https://doi.org/10.1099/00221287-136-12-2527.
22. Gomez, D., Peña Ccoa, W.J., Singh, Y., Rojas, E., and Hocky, G.M. (2021). Molecular paradigms for biological mechanosensing. J. Phys. Chem. B *125*, 12115–12124. https://doi.org/10.1021/acs.jpcb.1c06330.
23. Bieling, P., Li, T.D., Weichsel, J., McGorty, R., Jreij, P., Huang, B., Fletcher, D.A., and Mullins, R.D. (2016). Force feedback controls motor activity and mechanical properties of self-assembling branched actin networks. Cell *164*, 115–127. https://doi.org/10.1016/j.cell.2015.11.057.
24. Brogan, A.P., Bardetti, P., Rojas, E.R., and Rudner, D.Z. (2025). Cyclic-di-AMP modulates cellular turgor in response to defects in bacterial cell wall synthesis. Nat. Microbiol. *10*, 1698–1710. https://doi.org/10.1038/s41564-025-02027-2.
25. Storm, C., Pastore, J.J., MacKintosh, F.C., Lubensky, T.C., and Janmey, P.A. (2005). Nonlinear elasticity in biological gels. Nature *435*, 191–194. https://doi.org/10.1038/nature03521.
26. Williams, M.C., Reker, A.E., Margolis, S.R., Liao, J., Wiedmann, M., Rojas, E.R., and Meeske, A.J. (2023). Restriction endonuclease cleavage of phage DNA enables resuscitation from Cas13-induced bacterial dormancy. Nat. Microbiol. *8*, 400–409. https://doi.org/10.1038/s41564-022-01318-2.
27. Marquès-Bueno, M.D.M., Morao, A.K., Cayrel, A., Platre, M.P., Barberon, M., Caillieux, E., Colot, V., Jaillais, Y., Roudier, F., and Vert, G. (2016). A versatile multisite gateway-compatible promoter and transgenic line collection for cell type-specific functional genomics in Arabidopsis. Plant J. *85*, 320–333. https://doi.org/10.1111/tpj.13099.
28. Hammerschmidt, S., Wolff, S., Hocke, A., Rosseau, S., Müller, E., and Rohde, M. (2005). Illustration of pneumococcal polysaccharide capsule during adherence and invasion of epithelial cells. Infect. Immun. *73*, 4653–4667. https://doi.org/10.1128/IAI.73.8.4653-4667.2005.

STAR★METHODS

KEY RESOURCES TABLE

REAGENT or RESOURCE	SOURCE	IDENTIFIER
Bacterial and virus strains		
Bacillus subtilis PY79	Lab stock	N/A
Bacillus subtilis PY79 amyE::erm Pxyl-mreBCD, ΔmreBCD::spc PmreB-minCD	Garner Lab[20]	Strain ID: bMD545
Bacillus subtilis PY79 amyE:erm:phyperspank-SPOIIIJ-haloTag	Garner Lab	Strain ID: bZB112
Corynebacterium glutamicum	Theriot Lab	N/A
Escherichia coli MG1655	Lab Stock	N/A
Escherichia coli CG/pIV::25His	Sao-Jose Lab	N/A
Listeria seeligeri	Meeske Lab[26]	N/A
Chemicals, peptides, and recombinant proteins		
RADA	Tocris Bioscience	Cat. No. 6649
HADA	Tocris Bioscience	Cat. No. 6647
Ni Sepharose High Performance histidine-tagged protein purification resin	Cytiva	Cat. No. 17526802
Alexa Fluor 647 succinimidyl ester dye	ThermoFisher	Cat. No. A20006
Janelia Fluor 549 HaloTag Ligand	Promega	Cat. No. HT1020
Lysozyme	Millipore Sigma	Cat. No. L6876
N-lauroylsarcosine sodium salt	Millipore Sigma	Cat. No. L9150
Sorbitol	Millipore Sigma	Cat. No. 56755
Critical commercial assays		
HisTrap Desalting column	Cytiva	Cat. No. 17140801
CellASIC Microfluidic Plates for Bacteria	Millipore Sigma	Cat. No. B04A
ONIX Microfluidic Perfusion System	Millipore Sigma	Cat. No. CAX2-S0000
Experimental models: Organisms/strains		
Arabidopsis thaliana	Arabidopsis Biological Resource Center	Stock Number: CS2106156
Software and algorithms		
MATLAB	MathWorks	https://www.mathworks.com/
Custom MATLAB Image and Data Analysis Scripts	This work	https://github.com/TheRojasLab/Bardetti2025
Nikon Elements	Nikon	N/A

EXPERIMENTAL MODEL AND STUDY PARTICIPANT DETAILS

The following bacterial strains were used in this study:

Bacillus subtilis PY79

Genotype: domesticated wild-type. Source: lab stock.

B. subtilis bMD545

Genotype: *PY79 amyE::erm Pxyl-mreBCD, ΔmreBCD::spc PmreB-minCD*. Features: Xylose inducible induction of mreBCD operon. Source/reference: Garner Lab.[20]

B. subtilis bZB112

Genotype: *PY79 amyE:erm:phyperspank-SPOIIIJ-haloTag*. Features: IPTG inducible induction of SpoIIIJ-Halo Tag. Source: Garner Lab.

Corynebacterium glutamicum
Genotype: wild-type. Source: Theriot Lab.

Escherichia coli MG1655
Genotype: domesticated wild-type. Source: lab stock.

Listeria seeligeri
Genotype: wild-type. Source: Meeske Lab.[26]

Arabidopsis thaliana
Genotype: *pWOX5::H2B-2x-mCherry*. Features: Quiescent center expresses mCherry. Source: Birnbaum Lab.[27]

Culture Conditions
B. subtilis and *E. coli* strains were grown in Luria-Bertani (LB) medium at 37°C with shaking at 180 RPM. *Corynebacterium glutamicum* and *Listeria seelegeri* cells were grown in Brain Heart Infusion medium (BHI) at 30°C with shaking at 180 RPM. For induction of *Pxyl-mreBCD*, cells cultured overnight in LB supplemented with 3mM xylose were diluted in fresh media with the indicated amount of xylose until exponential phase. Hyperosmotic shocks were done using media supplemented with sorbitol. For hypoosmotic shocks, cells from overnight culture were back-diluted in media supplemented with 1M sorbitol and lower concentrations of sorbitol were used to shock the cells.

METHOD DETAILS

Light microscopy
All light microscopy was performed on a Nikon Eclipse Ti2 inverted fluorescence microscope with a sCMOS camera (BSI), controlled by Nikon Elements software, and equipped with an environmental chamber (Haison). An oil-immersion 100X object (NA 1.40) was used for imaging).

Spp1 endolysin purification
The bacteriophage endopeptidase, Spp1Lys, was purified by using a previously established protocol,[13] from *E. coli* strain CG/pIV::25His. Cells were grown at constant shaking at 28°C until an OD of 0.6-0.8, and then transferred to 42°C for 30 min and finally 16°C for 14 hours to induce protein expression. Cells were collected by centrifugation (4000 rpm for 30 min at 4°C) and resuspended in lysis buffer (20 mM Hepes, 500 mM NaCl, 20 mM imidazole, 1% glycerol and 1mM DTT, pH 6.5). Resuspended cells were lysed by sonication. The supernatant was collected after centrifugation (10000 rpm for 30 min at 4°C) and the enzyme was purified using a column packed with Ni Sepharose High Performance histidine-tagged protein purification resin. The elution buffer was the same as the lysis buffer except that the concentration of imidazole was 500 mM. The eluted fraction containing the purified protein was concentrated and the buffer was exchanged to a phosphate-based buffer (50 mM phosphate-Na, 500 mM NaCl, 25% glycerol, and 1 mM DTT, pH6.5) using a 5 mL HisTrap Desalting column. Whole extract, lysate, and eluted fractions were analyzed by SDS-PAGE and western blot. For western blot, proteins were transferred to a polyvinylidene difluoride membrane using Trans-Blot Turbo system (Biorad). For the detection of SPP1Lys an antibody against the His-tag was used and visualized with a ChemiDoc imaging System. Protein concentrations were determined using a nanodrop (ϵ= 32.89, M.W.=30.705). The purified enzymes were divided into small aliquots and kept at -80°C in the elution buffer.

Osmotic force-extension assays
To perform the osmotic-force-extension assay, consecutive osmotic shocks were performed using commercial microfluidic plates controlled by the ONIX microfluidic platform. Overnight cells were diluted in fresh media and grown until early exponential phase. Cells were then back-diluted into the loading well of the in the pre-warmed microfluidic plate and incubated for 30 min prior to the experiment. During this time the microfluidic channels and perfusion chamber were primed at a pressure of 4 psi. The cells were then loaded into the imaging chamber, and osmotic shocks were performed by perfusing media supplemented with sorbitol at a pressure of 8 psi. Osmotic shocks were performed every 5 min for a duration of 3 min each. Alexa Fluor 647 succinimidyl ester dye was used as a tracer dye to monitor media switching. To calculate the change in length resulting from osmotic shocks, for every cell, the longitudinal strain was calculated for during each osmotic shock, $\varepsilon_i = (l_f - l_i)/l_i$, where l_i is the length of the cell at the beginning of the interval and l_f is the maximum length of the cell during the interval.

Super-resolution measurement of single-cell width deformation
To perform single-cell measurements of circumferential strain the cell wall of *B. subtilis* was labeled with fluorescent D-amino acid RADA. Before the experiment, overnight cultures were back-diluted into fresh media and incubated until exponential phase was reached (OD 0.3-0.4). RADA was added to a concentration of 10 mM 1 hour before the start of the experiment. The same concentration of RADA was added to the cell loading well of a microfluidic chip. Images were taken 30 s before and 30 s after the osmotic shock.

Circumferential strain was measured using a super-resolution, fit-free method. Images of labeled single cells pre- and post-shock were computationally aligned by rotating them along their vertical axis. In each image, the sections of the cell wall not containing the septa were cropped, leaving only the cylindrical, sidewall section. Each image was then averaged along the vertical axis to obtain a single-cell average of the fluorescence profile across the width of the cell (Figure 1C). To calculate circumferential strain, pre- and post-shock profiles were normalized, one of them was scaled along the horizontal (width) axis at sub-pixel intervals, and then cross-correlated with the other profile.

The width distribution in Figure S1A was calculated by comparing the fluorescent profile of each cell from a population of cells to each other cell in the population. This resulted in a relative distribution of widths, which we calibrated using the established average cell width from the literature.

To measure the circumferential strain versus shock magnitude during dynamic relaxation of cell width (Figure 4D), first cell width versus time upon induction of the Rod complex was measured. To induce the Rod complex, an overnight culture induced with 3 mM xylose was back-diluted into a fresh media with 1mM xylose. The culture was grown to exponential phase before back-diluting it into LB supplemented with 10 mM xylose. Then, cell width was measured on LB agarose pads supplemented with 10 mM xylose every 20 minutes. The data revealed that cell width began decreasing within 15 minutes after the Rod complex induction (Figure 4A). Therefore, to measure circumferential strain upon osmotic shock during cell thinning, cells that had equilibrated to growth in 1 mM xylose were loaded into the perfusion chamber perfused with 10 mM xylose for 15 minutes prior to performing osmotic shocks. A similar protocol was used to measure lysis strain during width relaxation (see below).

To calculate the circumferential strain of the plasma membrane, the membrane was labeled by expressing a fusion between SpoIIIJ and a Halo tag. Strain bZB112 (*PY79 amyE:erm:phyperspank-SPOIIIJ-haloTag*) was grown overnight on an LB plate. The next day, a single colony was inoculated into 1 mL of LB supplemented with 5 μL IPTG to induce expression of the Halo-tagged protein. Cells were incubated until early exponential phase. One hour before the experiment, 200 nM of JaneliaFluor HaloTag 549 ligand was added to the culture. Osmotic shocks were performed using the protocol described above. The same concentration of the HaloTag ligand was added to the loading well of the microfluidic device.

To measure changes in cell width in *C. glutamicum* and *L. selegerii*, 0.5 mM of RADA was used to label the cells 1 hour before the experiments. For *E. coli* MG1655, the cell wall was labelled with HADA for 1 hour. Osmotic shocks were performed using the same protocol described above.

Hydrolysis assay

Hydrolysis experiments were performed in microfluidic devices at 37C. Lysozyme (Sigma Aldrich) was dissolved in the desired media before the experiments. Purified Spp1 was added directly to the media in the designated chamber at the indicated concentration. Cells were grown in rich media in the perfusion chamber for 5 minutes prior to the perfusion of the hydrolase. To control for cell lysis, 0.1μM of propidium iodide (Sigma Aldrich) was added to the media with the enzymes. To measure changes in width and length, images were taken 1 minute before and after adding the enzymes.

Derivation of Equation 1 and theoretical phase space

Two-dimensional linear elasticity with no shear is given by

$$\begin{pmatrix} \lambda_l \\ \lambda_\theta \end{pmatrix} = \begin{pmatrix} E_l & E_{l\theta} \\ E_{l\theta} & E_\theta \end{pmatrix} \begin{pmatrix} \varepsilon_l \\ \varepsilon_\theta \end{pmatrix}$$

where E_l and E_θ are the principal elastic moduli and $E_{l\theta}$ is the modulus that couples deformation in the principal directions. Inverting this equation gives

$$\begin{pmatrix} \varepsilon_l \\ \varepsilon_\theta \end{pmatrix} = \frac{1}{E_l E_\theta - E_{l\theta}^2} \begin{pmatrix} E_\theta & -E_{l\theta} \\ -E_{l\theta} & E_l \end{pmatrix} \begin{pmatrix} \lambda_l \\ \lambda_\theta \end{pmatrix}$$

Substituting $\nu = E_{l\theta}/E_\theta$ and $\alpha = E_\theta/E_l$ to eliminate $E_{l\theta}$ and E_θ yields Equation 1 of the main text:

$$\begin{pmatrix} \varepsilon_l \\ \varepsilon_\theta \end{pmatrix} = \frac{1}{E_l} \frac{1}{\alpha(\alpha^{-1} - \nu^2)} \begin{pmatrix} 1 & -\nu \\ -\nu & \alpha^{-1} \end{pmatrix} \begin{pmatrix} \lambda_l \\ \lambda_\theta \end{pmatrix}$$

Note that in Equation 1 the non-dimensional Poisson ratio, ν, was not defined in the traditional manner ($E_{l\theta}/E$) since the cell wall is anisotropic and there are two options for how to define it: $E_{l\theta}/E_l$ or $E_{l\theta}/E_\theta$. Arbitrarily defining it as $E_{l\theta}/E_l$ leads to the non-dimensional diagonal element that appears in Equation 1. Using the alternate definition does not affect the analysis. The boundary between the finger trap regime and the no-finger trap regime comes from solving Equation 1 for the condition $\varepsilon_\theta = 0$. The condition that $\alpha^{-1} > \nu^2$ results from imposing the physicality condition that the determinant, $E_l E_\theta - E_{l\theta}^2$, be positive. Note that this constraint only strictly applies in the limit of the thin shell approximation, which is likely to be approximately true for *B. subtilis* since the thickness of the cell wall is ≈40nm and the radius of the cell is ≈400nm. Contributions of normal stress to the balance of turgor pressure would shift this boundary.

The slices through parameter space that constrain the mechanical properties of the low pressure, finger trap, and stress-softened regimes were found by first finding the slopes of the regression to the circumferential strain versus shock magnitude in the three

regimes (slopes m_θ of dotted lines in Figure 2D), and then substituting these as well as the slope of the regression to longitudinal strain versus shock magnitude, ml into Equation 1 as $\varepsilon_{l,\theta} = m_{l,\theta}\Delta C_{out}$. This assumes that in each of these three regimes the cell wall is a linear material near an appropriate reference state. Rather than assuming that the material is linear globally (it obviously is not) this analysis is simply a way to estimate the relative local mechanical properties in the three regimes. Furthermore, all materials are linear for small deformations and non-linear for large deformations, and whether the reference state is the rest state need not affect whether the material behaves locally like a linear elastic material with given parameters α and ν.

Cell lysis assay

To measure changes in dimensions in response to lysis, cells were lysed with 5% N-lauroylsarcosine sodium salt. The cell depleted of the turgor pressure shrank to its rest length. To measure the change in length in response to lysis, images were taken 1 min before the addition of the detergent and after the detergent was washed away using LB. To calculate changes in dimensions for different levels of Rod complex induction, cells grown overnight in LB with 5 mM xylose were back diluted in LB supplemented with 0.5 mM, 5 mM, or 30 mM xylose. The same xylose concentrations were added to the media with detergent and the washing media.

Pressure measurements

To measure pressure, osmotic force extension experiments were combined with measurements of lysis strains. Pressure was calculated empirically as the hyperosmotic shock magnitude that caused contraction of the cell wall to the rest length observed upon lysis. This was found by finding the intercept of the lysis strain with the regression of the two data points from the osmotic force-extension curve that were immediately above and below the lysis strain. Error in pressure was propagated from the s.e.m. of the lysis strains and the standard error of regression of the osmotic force-extension data points.

Mathematical model of cell morphogenesis

To model morphogenesis of a rod-shaped cell where width could change dynamically, we considered a cylindrical cell wall with a constant thickness of 40 nm and pressure of 10 atm. To balance pressure, making the thin-shell approximation, the total longitudinal tension borne by the cell wall is $\lambda_l = \frac{PR}{2}$ and the circumferential tension is $\lambda_\theta = PR$. We discretized the cell wall into 100 layers and allowed the stress and strain to vary across the thickness of the cell wall given these global force-balance constraints. To model dynamic growth and morphogenesis of the cell, we defined an arbitrarily small time step. During each time step we removed one layer (1/100th of wall thickness) from the outer surface of the cell wall and added a unstretched layer to the inner surface of the wall, and then allowed the cell wall to deform to satisfy the global force balance constraints using a standard energy minimization routine.

Transmission electron microscopy

Transmission electron microscopy of thin sections of formaldehyde-fixed freeze-substituted B. subtilis cells was performed as follows. An overnight culture of wild-type B. subtilis was back-diluted into 5 mL of LB and incubated at 37 °C with shaking for 2.5 hours. 2 x 1 mL of culture was transferred to 1.5 mL tubes containing either 1 mL pre-warmed LB or 1 mL pre-warmed LB+1 M sorbitol (to apply 500 mM hyperosmotic shock). Cultures were briefly vortexed and then spun for 4 min at 3500 RPM. Supernatant was removed and pellet was re-suspended in 600 mL PBS to wash, spun 4 min at 3500 RPM, and resuspended in 1ml LRR fixative solution[28] (0.5 mL 0.15% ruthenium red, 125 µL 16% formaldehyde, 0.0155 g lysine acetate (Sigma); distilled water to 1 mL).

Samples were then subjected to high pressure freezing and freeze substitution. 3 mm planchette with 100 mm deep were lightly coated with hexadecene before being filled with approximately 1.2mL of fixed sample. An absorbent filter paper was used to soak out extra liquid, and then the sample was slightly dry for ~ 5 min. The hats were then sealed in the planchette holder for high-pressure freezing (Leica ICE High Pressure Freezing Platform, Leica Microsystems). The frozen samples were immediately transferred into liquid nitrogen and then into cryovials containing freeze substitution solutions (2-ml cryovials (Nalgene) containing 2% (wt/vol) osmium tetroxide (OsO_4) and 0.1% (wt/vol) uranyl acetate in anhydrous acetone with 0.075% (wt/vol) ruthenium red and 2% H_2O) under liquid nitrogen temperature. The samples were brought into a Leica AFS2 EM freeze substitution unit (Leica Microsystems) and left in the -90°C for 79 hours. Since the acetone:osmium mixture liquifies at -90°C, the hats were slowly submerged in the freeze substitution media. The temperature of the unit was raised 5°C per hour to –60°C and incubated for 12 hours, then to –30°C for an additional 6 hours, and finally to a temperature of 0°C for 6 hrs.

After removal from freeze substitution unit, samples were washed in pure ethanol 3 x 1 hour on ice to rinse out osmium. They were then washed with 1:1 100% ethanol:LR White for 2 hours on ice, 1:2 100% ethanol:LR White overnight at 4°C, pure LR White for 8 hours on ice, and finally pure LR White overnight at 4°C. Samples were then embedded in gelatin capsules filled with LR White at room temperature and polymerized for 48 hours at 55–60 °C. Thin sections were cut onto 200 mesh grids and counterstained with 4% aqueous uranyl acetate for 5 min. Stained grids were examined under JEOL1400 Flash transmission electron microscope (Japan) and photographed with a Gatan Rio 16 camera (Gatan Inc. Pleasanton, CA). All chemicals and EM grids are purchased from Electron Microscopy Sciences Hatfield, PA.

Osmotic shocks on Arabidopsis roots

Arabidopsis thaliana (Col-0 ecotype) plants carrying the transgenic reporter, pWOX5::H2B-2x-mCherry,[27] were used. Seeds were stratified at 4℃ for 2 days, sterilized, placed on agar plates containing 0.5X Murashige and Skoog (MS) salts (Sigma M5524),

0.5% (w/v) sucrose (Sigma S0389). Plates were grown vertically in growth chambers at 22°C under long-day conditions (16 h light/8 h dark).

For hyperosmotic shock experiments, roots were placed on a glass slide with liquid ½ MS with 0.5% (w/v) sucrose media (liquid 0.5X MS) and imaged using a Zeiss LSM800. The media was then replaced with liquid ½0.5X MS with 0.5 M D-Mannitol (Sigma M4125) to induce a hyperosmotic shock and re-imaged.

For hypoosmotic shock experiments, roots were initially placed in liquid 0.5X MS with 0.5 M D-Mannitol for 1 hour, then imaged in the same medium. After imaging the media was replaced with liquid 0.5X MS to induce a hypoosmotic shock, and roots were re-imaged.

For width (radial) measurements, the pWOX5-labeled quiescent center (QC) was used as a central reference point, and distances were measured from the QC to the outermost cell files on both the left and right sides of the root. For longitudinal strain measurements, distances were measured from the QC to the root tip.

QUANTIFICATION AND STATISTICAL ANALYSIS

Statistical tests for comparisons, *p-value*s, precision measures, all *n* numbers, and their meanings, are found in the figure legends. Comparisons were deemed significant if the $p<0.05$.

Current Biology, Volume *36*

Supplemental Information

Non-linear stress-softening of peptidoglycan mediates bacterial cell shape homeostasis

Paola Bardetti, Felix Barber, Dylan Fitzmaurice, and Enrique R. Rojas

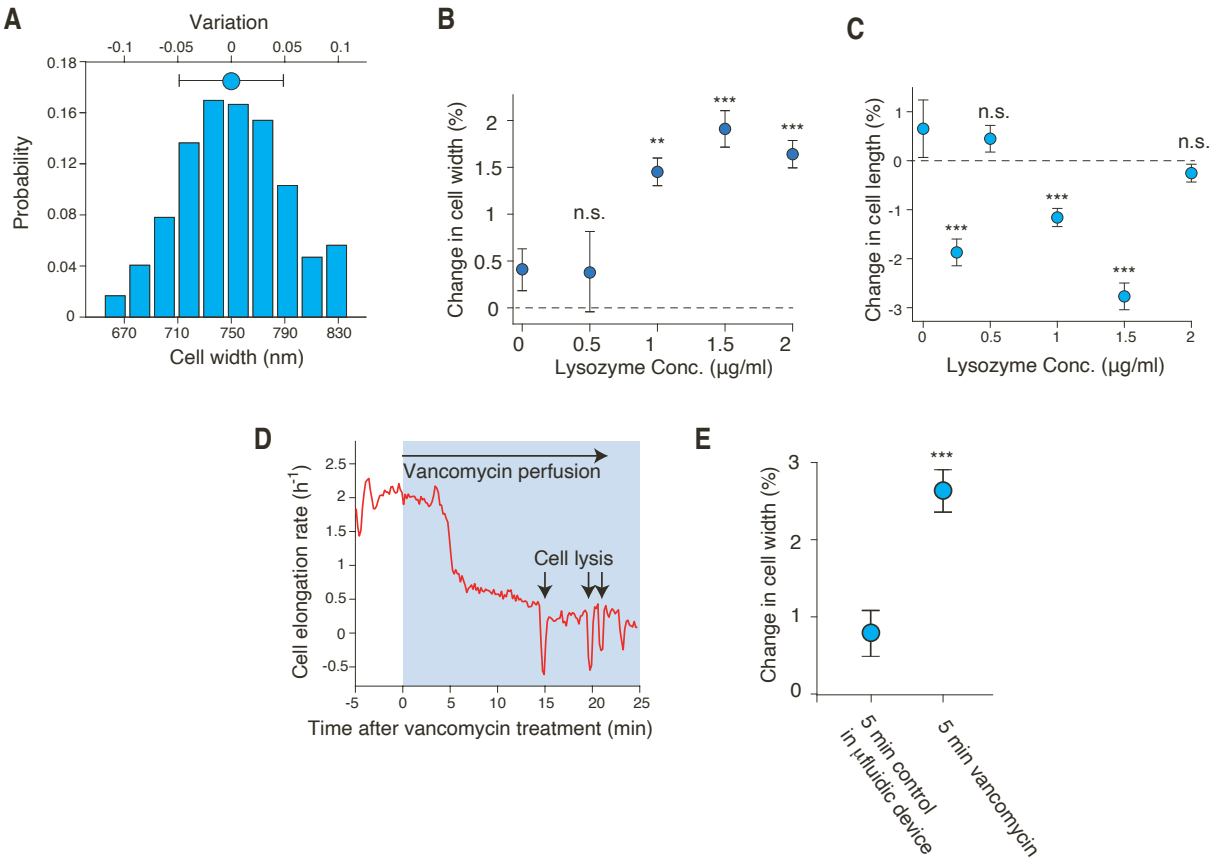

Figure S1. Lysozyme and vancomycin treatment cause cell widening. Related to Figure 1. A) Distribution of cell width as calculated using the super-resolution method developed in this study. n=31 cells. Error bars indicate +/- 1 s.d. B) Mean change in cell width upon lysozyme treatment. Error bars indicate +/- 1 s.e.m. B) Mean change in cell length upon lysozyme treatment, controlling for cell growth. Error bars indicate +/- 1 s.e.m. D) Population-averaged cellular elongation rate versus time during acute perfusion with 10 mg/mL vancomycin. n=18 cells across 1 experiment. E) Change in cell width during 5 minutes of growth in the microfluidic chip (control) and during 5 minutes of treatment with 10 µg/mL vancomycin. ***: $p<10^{-4}$, student two-sided t-test (STSTT) compared to untreated control.

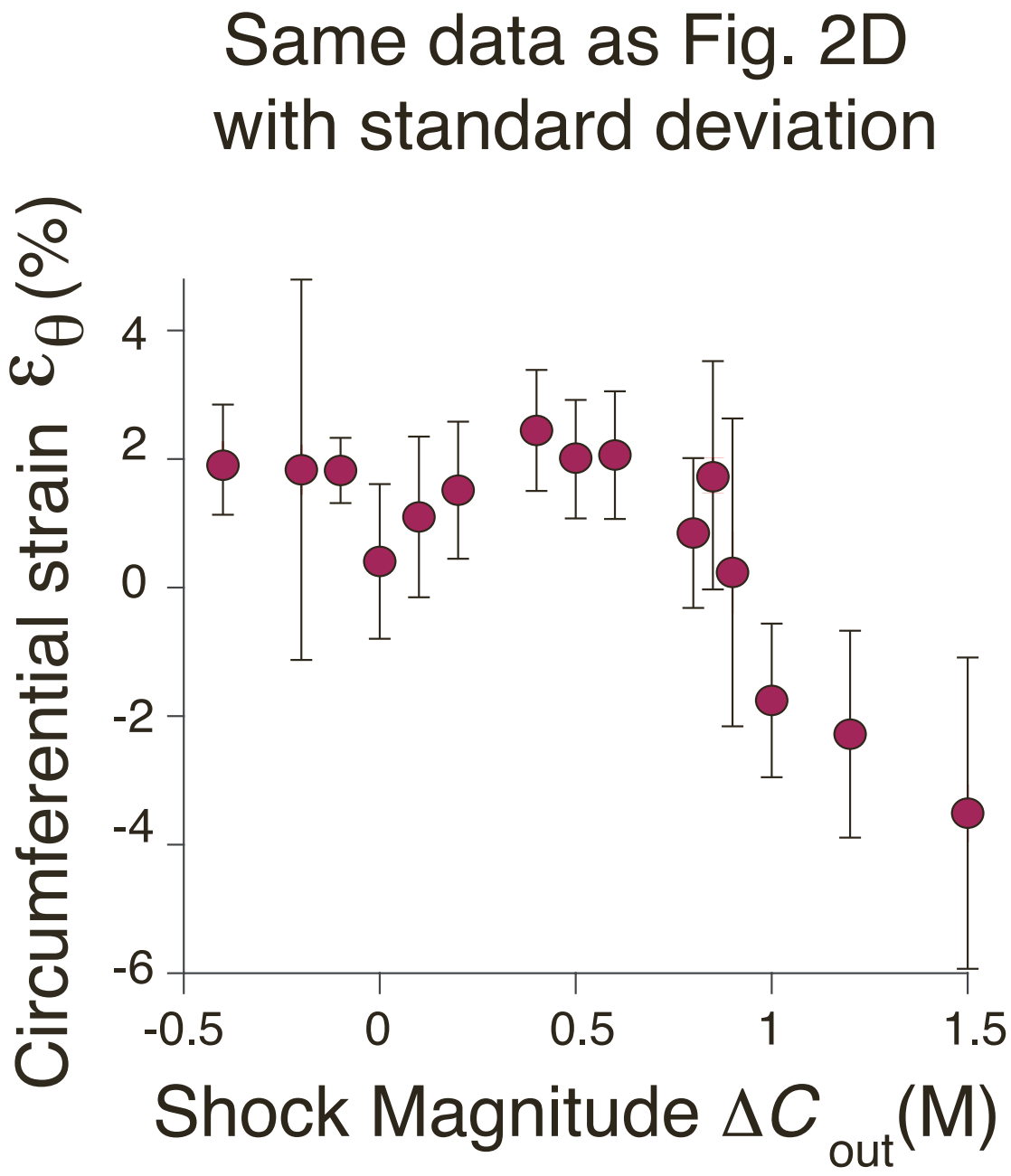

Figure S2. Circumferential strain is resolved to within +/- 1%. Related to Figure 2.
The same data as in Fig. 2D of the main text except where error bars respresent +/- 1 s.d.

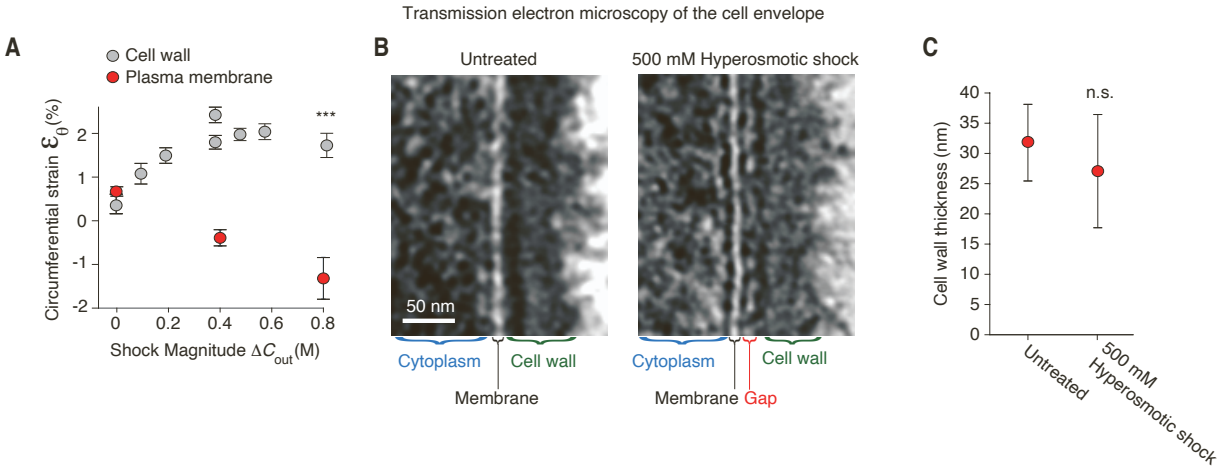

Figure S3. The plasma membrane constricts upon modest hyperosmotic shock. Related to Figure 2.

A) Circumferential strain versus shock magnitude across several osmotic force extension experiments, as measured by tracking the plasma membrane (red circles). The membrane was labeled by expressing a fusion between SPOIIJ and a HALO tag (Table S1). n=25-40 cells across 1 replicate experiments per shock magnitude. Error bars: +/- 1 s.e.m. The gray circles show the circumferential strain calculated by tracking the cell wall, which is the same data shown in Fig. 2D of the main text. ***: $p<10^{-4}$ STSTT comparing cell wall and plasma membrane deformation . B) Transmission electron microscopy of the cell envelope before and after 500 mM hyperosmotic shock. C) Thickness of the cell wall before and after 500 mM hyperosmotic shock. n=10 cell wall segments for each condition. Error bars represent +/- 1 s.d. n.s.: not significant compared to untreated control.

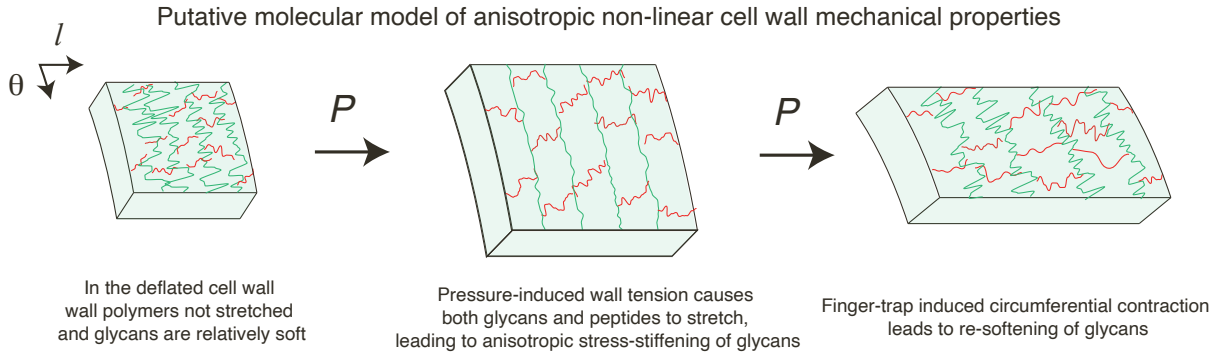

Figure S4. Putative qualitative molecular model of the anisotropic non-linear cell wall mechanical properties. Related to Figure 2.

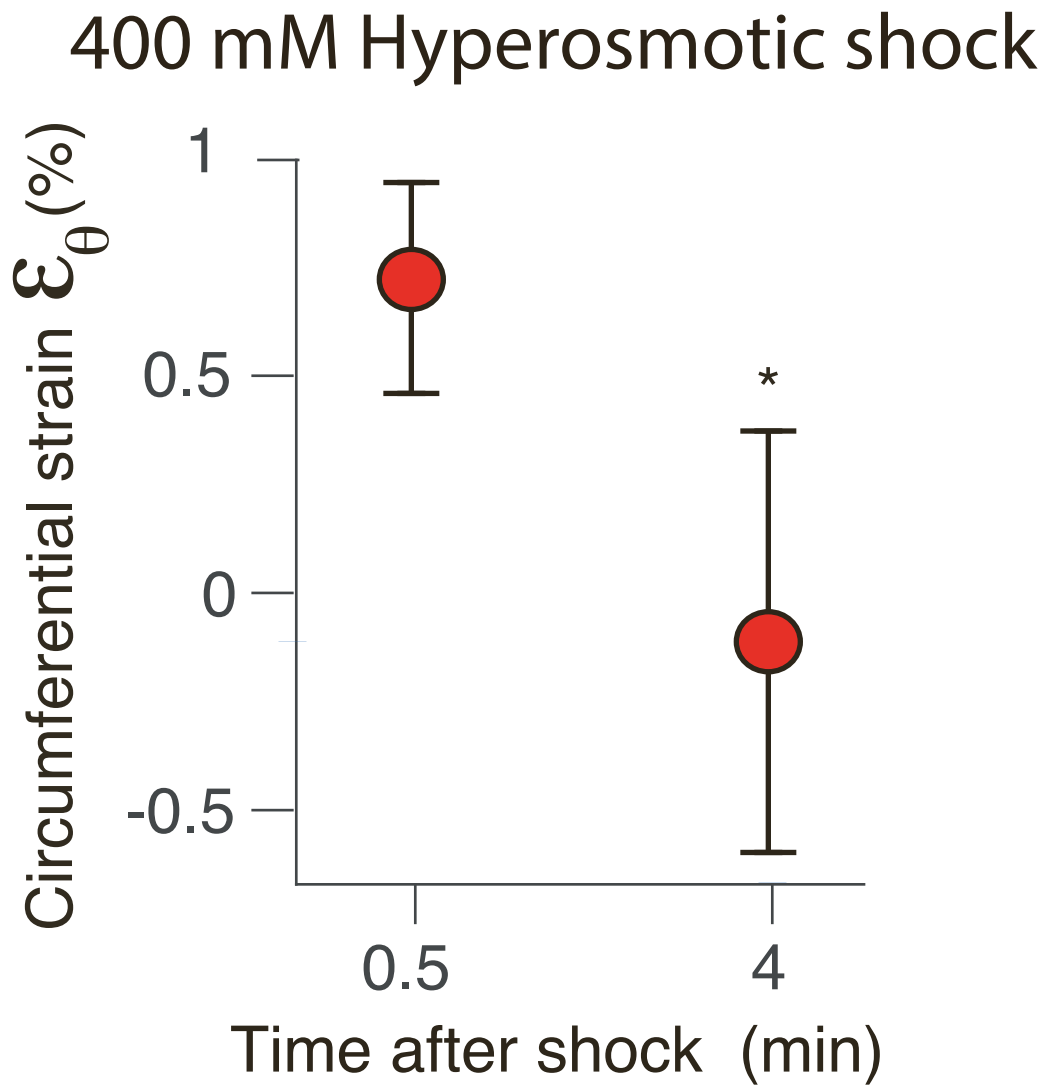

Figure S5. Finger trap deformation is transient. Related to Figure 2.
Circumferential strain upon a 400 mM hyperosmotic shock, as measured 30 s and 2 min after the shock, demonstrating that finger trap deformation is transient, as predicted by our model. For these experiments, the absolute circumferential strain was corrected by subtracting the circumferential strain caused by growth in the microfluidic chip for the same amount of time. n=27 and 22 cells across one experiment for 0.5 and 5 minute measurements, respectively. Error bars represent +/- 1 s.e.m. ***: $p<10^{-2}$, STSTT compared to standard 0.5 minute measurement.